

## Fringe electric fields of flat and cylindrical deflectors in electrostatic charged particle storage rings

E. M. Metodiev,<sup>1,2,3,4</sup> K. L. Huang,<sup>1,2</sup> Y. K. Semertzidis,<sup>1,3,4</sup> and W. M. Morse<sup>1</sup>

<sup>1</sup>*Department of Physics, Brookhaven National Laboratory, Upton, New York 11973, USA*

<sup>2</sup>*Harvard College, Harvard University, Cambridge, Massachusetts 02138, USA*

<sup>3</sup>*Center for Axion and Precision Physics Research, IBS, Daejeon 305-701, Republic of Korea*

<sup>4</sup>*Department of Physics, KAIST, Daejeon 305-701, Republic of Korea*

(Received 10 September 2013; revised manuscript received 13 June 2014; published 18 July 2014)

Analytic expressions for the potentials and fields of flat and cylindrical plates, including the fringe fields, are given. The present analysis extends and simplifies the current expression for the fields of flat plates and develops expressions for the fringe fields of cylindrical plates in terms of polar coordinates. The development of a FORTRAN program to output the field strength at a given location within the Proton Electric Dipole Moment (Proton EDM) ring is then described. Fourth-order Runge-Kutta integration is used to investigate the effect of fringe fields on particle and spin dynamics with precision tracking in the proposed Proton EDM experiment.

DOI: [10.1103/PhysRevSTAB.17.074002](https://doi.org/10.1103/PhysRevSTAB.17.074002)

PACS numbers: 41.20.-q, 29.20.db, 21.10.Ky, 02.60.-x

### I. INTRODUCTION

Fringe fields are often neglected in analysis of electrostatic configurations. The hard-edge approximation that is often used accounts for the energy change of a particle through the fringe region and does not include the fringe fields themselves. However, this cannot be the full story since the hard-edge fields are not solutions to the Maxwell equations for the given system.

To fully account for the effect of fringe fields, an analytic expression for the fringe electric fields is crucial. We begin with the studied case of the fringe fields near flat electrode plates, and then we discuss the results extended to cylindrical electrodes using conformal mappings consistent with the cylindrical geometry.

We take the problems to be two-dimensional, with the plates extending infinitely far in the third direction. We arrive at analytic expressions for the fringe fields of finite flat and cylindrical plates, which we then simplify through the introduction of several complex functions.

Finally, we describe the implementation of the mathematical expressions of the fringe fields into a FORTRAN tracking program using fourth-order Runge-Kutta integration. We intend for this to become a valuable tool in accurately determining the effects of fringe fields on particle and spin dynamics in the fringe regions through precision tracking.

### II. FLAT PLATES

The first analysis of fringe fields of finite flat plates was done by Maxwell [1]. An implicit mapping defines the electric field at the fringes of flat plates charged at  $+V_0$  and  $-V_0$ , namely,

$$x = \frac{d}{2\pi}(u + 1 + e^u \cos v), \quad y = \frac{d}{2\pi}(v + e^u \sin v), \quad (1)$$

where  $v \in (-\pi, \pi)$  and  $u \in (-\infty, \infty)$ , and  $d$  is the spacing between the plates. The direction perpendicular to the plates is the  $y$  direction, and the longitudinal direction is the  $x$  direction.

Using this parametric definition, the implicitly defined coordinate  $v(x, y)$  is the normalized potential such that  $v(x, y) = \pi V(x, y)/V_0$ . The uniqueness theorem then guarantees that the electric field must follow from this potential.

The resulting transverse field  $E_y$  and longitudinal field  $E_x$  are given by the following expressions:

$$E_x = \frac{2V_0}{d} \frac{e^u \sin v}{(1 + 2e^u \cos v + e^{2u})}, \quad (2)$$

$$E_y = -\frac{2V_0}{d} \frac{1 + e^u \cos v}{(1 + 2e^u \cos v + e^{2u})}. \quad (3)$$

The two electric field components can be expressed as  $E_x = E \sin \phi$  and  $E_y = E \cos \phi$ , where

$$E = -\frac{2V_0}{d} \frac{1}{\sqrt{1 + 2e^u \cos v + e^{2u}}} \quad (4)$$

and

---

Published by the American Physical Society under the terms of the *Creative Commons Attribution 3.0 License*. Further distribution of this work must maintain attribution to the author(s) and the published article's title, journal citation, and DOI.

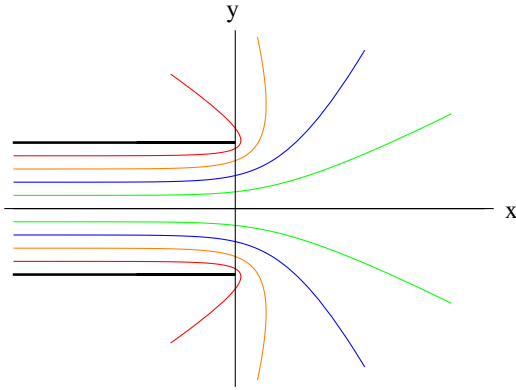


FIG. 1. Equipotential lines, equally spaced in voltage, at the fringes of flat parallel plates.

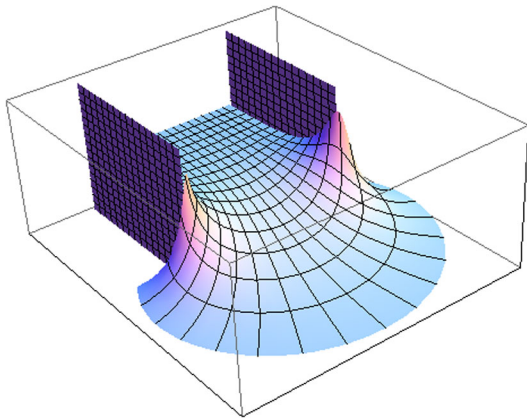


FIG. 2. The magnitude of the electric field  $|E|$  between finite parallel flat plates. The  $x$  and  $y$  directions are spatial dimensions and the vertical represents the electric field strength.

$$\phi = \arctan\left(\frac{\frac{\partial x}{\partial v}}{\frac{\partial y}{\partial v}}\right) = \arctan\left(\frac{-e^u \sin v}{1 + e^u \cos v}\right). \quad (5)$$

Fixing  $v$  and varying  $u$  gives a parametric method of plotting equipotential lines from the analytic expression. Figure 1 demonstrates the equipotential lines for evenly spaced potentials between  $+V_0$  and  $-V_0$  using the implicit functions given above.

Thus we have determined the expressions for the radial and longitudinal fields,  $E_x$  and  $E_y$ , of flat parallel plates in terms of  $u$  and  $v$ . The resulting electric field is shown in Fig. 2.

### III. CYLINDRICAL PLATES

Doskeyev *et al.* [2] in 2011 gave similar implicit analytic mappings for finite cylindrical plates that terminate at  $\psi = 0$ , neglecting the other end. Given in cylindrical

coordinates  $(\rho, \psi)$  concentric with the plates, the expressions are

$$\rho = \sqrt{R_1 R_2} \exp\left[\frac{1}{2\pi} \ln \frac{R_2}{R_1} (e^u \sin v + v)\right], \quad (6)$$

$$\psi = \frac{1}{2\pi} \ln \frac{R_2}{R_1} (1 + e^u \cos v + u), \quad (7)$$

where  $v \in (-\pi, \pi)$  and  $u \in (-\infty, \infty)$ , and  $R_1$  and  $R_2$  are the inner and outer radii, respectively. Using this parametric definition, the equipotential lines for an illustrative case of deflectors forming a half circle were plotted using *Mathematica*. Figure 3 depicts the equipotential lines for evenly spaced potentials between  $+V_0$  and  $-V_0$  for the cylindrical plates. The two cylindrical ends were taken to be sufficiently far apart so that the solutions for each end could be added directly.

At  $v = \pm\pi$  we have that  $\rho = R_1$  or  $\rho = R_2$ , and  $\psi$  ranges over  $\psi \leq 0$  as  $u$  ranges from  $-\infty$  to  $+\infty$ . These conditions give the correct equipotential geometry for  $+V_0$  on the outer plate and  $-V_0$  on the inner plate, and we see that  $\nabla^2 v = 0$  by implicitly differentiating. This check can be done by confirming that  $u$  and  $v$  satisfy the Cauchy-Riemann conditions and thus Laplace's equation [3]. The uniqueness theorem thus guarantees that  $V(\rho, \psi) = \frac{V_0}{\pi} v(\rho, \psi)$  is the potential for the cylindrical plate configuration, giving the desired fringe fields.

From this, the electric field can be found by implicitly differentiating, yielding

$$\vec{E} = -\nabla V = -\frac{V_0}{\pi} \left( \frac{\partial v}{\partial \rho}, \frac{1}{\rho} \frac{\partial v}{\partial \psi} \right). \quad (8)$$

With this method, we can determine the two components of the electric field,  $E_\rho$  and  $E_\psi$ . Differentiating the potential gives

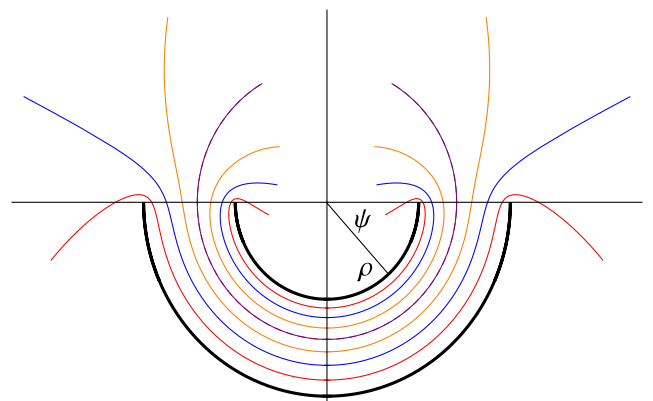


FIG. 3. Equipotential lines, equally spaced in voltage, of concentric semicircles found using the methods mentioned [2] for cylindrical plates by reflecting about the vertical axis. Figure shown is for semicircular plates where  $R_2/R_1 = 2$ .

$$E_\rho = -\frac{2V_0(1 + e^u \cos v) \exp[-\frac{1}{2\pi} \ln \frac{R_2}{R_1} (e^u \sin v + v)]}{\ln(\frac{R_2}{R_1}) \sqrt{R_1 R_2} (1 + 2e^u \cos v + e^{2u})}, \quad (9)$$

$$E_\psi = \frac{2V_0 e^u \sin v \exp[-\frac{1}{2\pi} \ln \frac{R_2}{R_1} (e^u \sin v + v)]}{\ln(\frac{R_2}{R_1}) \sqrt{R_1 R_2} (1 + 2e^u \cos v + e^{2u})}. \quad (10)$$

The expressions above can be represented, like the field expressions for the flat plates, in a further simplified form. We take  $E$  to be the negatively signed magnitude of the electric field:

$$E = -\frac{2V_0 \exp[-\frac{1}{2\pi} \ln \frac{R_2}{R_1} (e^u \sin v + v)]}{\ln(\frac{R_2}{R_1}) \sqrt{R_1 R_2} \sqrt{1 + 2e^u \cos v + e^{2u}}}. \quad (11)$$

Then the two components of the field can be written in the following way:

$$E_\rho = E \cos \phi, \quad (12)$$

$$E_\psi = E \sin \phi, \quad (13)$$

where

$$\phi = \arctan\left(\frac{-e^u \sin v}{1 + e^u \cos v}\right). \quad (14)$$

Thus we have determined the electric field components  $E_\rho$  and  $E_\psi$  of cylindrical parallel plates in terms of  $u$  and  $v$ . The field expressions can be used to determine particle dynamics through the fringe electric field regions for the

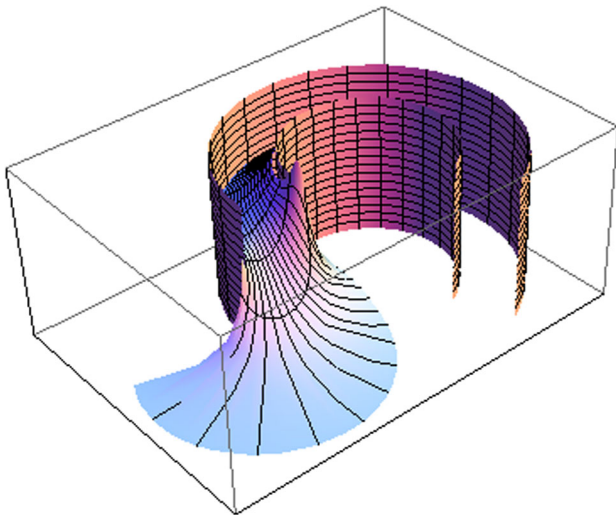


FIG. 4. The magnitude of the electric field  $|E|$  between finite cylindrical plates. The  $x$  and  $y$  directions are spatial dimensions and the vertical represents the electric field strength. The standard field between the cylindrical shells is shown in the back, with the fringe effect occurring at the front of the image.

Proton Electric Dipole Moment (EDM) experiment through precision tracking.

A graph of the electric field strength was made using *Mathematica* in order to illustrate the above result. The depiction gives a clearer picture of the equipotential surfaces as well as of the fringe field strength. The strength of the fringe electric fields due to finite cylindrical plates is shown in Fig. 4.

The equipotential surfaces of the cylindrical plates can be used to shape the end of the cylindrical plates of the Proton EDM experiment, similar to the Rogowski profile [4] used for flat plates. The analytic expressions of these surfaces are given in this section parametrically.

#### IV. COORDINATE MAPPING INVERSION

The coordinate mapping that gives  $u$  and  $v$  is illustrated in Fig. 5. The circulating lines represent lines of constant  $v$  and the lines that end normal to the cylindrical plates represent lines of constant  $u$ .

To invert this mapping, first we establish the equivalence of the  $(x, y)$  and  $(\rho, \psi)$  mappings in terms of  $u$  and  $v$  by noting that the  $(\psi, \ln[\rho/\sqrt{R_1 R_2}])$  mapping is equivalent to the  $(x, y)$  mapping up to a scaling constant. Thus we will invert the  $(x, y)$  mapping, which will then be simply related to the  $(\rho, \psi)$  mapping.

We define  $z = x + iy$  and  $w = u + iv$ . Multiplying the  $y$  expression in Eq. (1) by  $i$  and adding it to the  $x$  expression yields

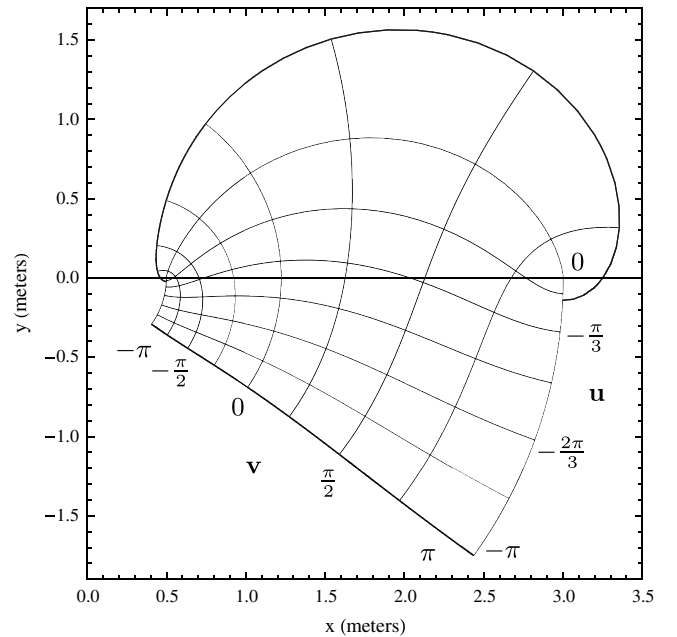


FIG. 5. Lines of equally spaced constant  $u$  and  $v$  values of the cylindrical coordinate mapping for radii  $R_1 = 0.5$  m and  $R_2 = 3.0$  m.

$$z = \frac{d}{(2\pi)}(1 + w + e^w). \quad (15)$$

Using the condition that  $-\pi < v < \pi$ , this equation can be solved for  $w$  as

$$w = -1 + \frac{2\pi}{d}z - W_{\kappa(z)} \left[ \exp \left( -1 + \frac{2\pi}{d}z \right) \right], \quad (16)$$

where  $W_{\kappa(z)}$  is the  $\kappa(z) = \lceil \frac{\Im(2\pi z) - \pi}{2\pi} \rceil$  branch of the Lambert  $W$  function [5] defined so that  $z = W(z) \exp[W(z)]$ .  $\lceil z \rceil$  is the ceiling function and  $\Im(z)$  takes the imaginary part of the argument. Henceforth, we will write  $W_{\kappa(z)} \equiv W$ .

Taking real and imaginary parts gives the desired expressions for  $u(x, y)$  and  $v(x, y)$  for the flat finite plates, namely,

$$u = -1 + \frac{2\pi}{d}x - \Re \left( W \left\{ \exp \left[ -1 + \frac{2\pi}{d}(x + iy) \right] \right\} \right), \quad (17)$$

$$v = \frac{2\pi}{d}y - \Im \left( W \left\{ \exp \left[ -1 + \frac{2\pi}{d}(x + iy) \right] \right\} \right), \quad (18)$$

where  $\Re$  takes the real part and  $\Im$  takes the imaginary part of the argument.

Now we solve for  $u(\rho, \psi)$  and  $v(\rho, \psi)$  in the same way through the equivalence described above. We thus arrive at the  $u$  and  $v$  expressions for the finite cylindrical plates:

$$u = \Re \left\{ -1 + \frac{2\pi z}{\ln(\frac{R_2}{R_1})} - W \left[ \exp \left( -1 + \frac{2\pi z}{\ln(\frac{R_2}{R_1})} \right) \right] \right\}, \quad (19)$$

$$v = \Im \left\{ -1 + \frac{2\pi z}{\ln(\frac{R_2}{R_1})} - W \left[ \exp \left( -1 + \frac{2\pi z}{\ln(\frac{R_2}{R_1})} \right) \right] \right\}, \quad (20)$$

where  $z = \psi + i \ln(\rho / \sqrt{R_1 R_2})$  and the branch of the Lambert  $W$  function is  $\kappa(z) = \lceil [\Im(\frac{2\pi z}{\ln(R_2/R_1)}) - \pi] / 2\pi \rceil$ .

Thus we have extended the expression for the electric field of finite cylindrical plates to a closed form in cylindrical coordinates by substituting  $u$  and  $v$  in  $E_\rho$  and  $E_\psi$ . These expressions were checked graphically and analytically for both the flat and cylindrical geometries.

## V. PROTON EDM EXPERIMENT

### A. Proton EDM geometry

The Proton EDM experiment [6] proposes to measure the electric dipole moment of the proton with a sensitivity of  $10^{-29} e \cdot \text{cm}$ . The design uses protons at the magic momentum of  $p_0 = 0.7 \text{ GeV}/c$  in an all-electric storage ring with a momentum spread of  $(dp/p_0)_{\text{rms}} = 10^{-4}$ .

The Proton EDM storage ring geometry [6], shown in Fig. 6, consists of 16 sections of concentric cylindrical

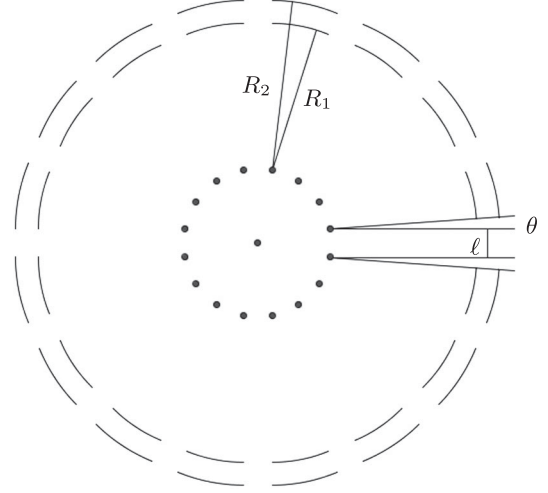


FIG. 6. The Proton EDM storage ring geometry. The ring consists of 16 sections of concentric cylindrical deflectors separated by some distance  $\ell$ . Each section spans  $2\pi/16 - 2\theta$  radians. The fringe effects occur near the ends of the deflectors.

deflectors of radii  $R_1$  and  $R_2$  each spanning  $2\pi/16 - 2\theta$  rad separated by straight sections of length  $\ell$ . The outer circumference of the lattice is then  $2\pi R_2 + 16\ell$ . The currently considered parameters used in the following analysis are  $R_1 = 39.985 \text{ m}$ ,  $R_2 = 40.015 \text{ m}$ , and  $\ell = 2.0 \text{ m}$ . The potentials on the plates are chosen such that the electric field is  $10.5 \text{ MV/m}$  exactly between the two plates.

The geometry is treated as two dimensional, neglecting the vertical dimension. In the Proton EDM experiment, vertical focusing will be provided by electrostatic quadrupoles in the straight sections. The quadrupoles are not included in the simulation since the vertical dimension of the problem is neglected. The tracking simulation focuses on the effects of the fringe fields of the deflectors.

An important feature of the geometry is its reflectional symmetry. The origin of coordinates is chosen to be at the center of the ring. The fringe regions of interest occur at the ends of the deflectors. The expressions for the electric field of the deflectors, developed in the previous section, were applied to determine the electric field at all points in the ring.

### B. Program implementation

The Lambert  $W$  function is implemented by a convergent sequence defined by Halley's method [7] that converges to  $W_{\kappa(z)}(z)$  for a given  $z$ . The sequence used takes the form

$$w_{n+1} = w_n - \frac{w_n e^{w_n} - z}{e^{w_n}(w_n + 1) - \frac{(w_n + 2)(w_n e^{w_n} - z)}{2w_n + 2}}. \quad (21)$$

In the expressions for  $u$  and  $v$  occurs the term  $W\{\exp[-1 + 2\pi z / \ln(R_2/R_1)]\}$ . Analytically, there is no trouble in working with that term. However,  $\Re(z) > 1000$

risks overflow in computation and limits the utility of the analytic mapping. This issue motivates the introduction of another function.

The Wright  $\omega$  function [8] is defined such that

$$\omega(z) = W_{\kappa(z)}(\exp(z)), \quad (22)$$

where the branch is  $\kappa(z) = \lceil (\Im(z) - \pi)/2\pi \rceil$ .

If we define  $s = -1 + 2\pi z / \ln(R_2/R_1)$ , then using the  $\omega$  function,  $u$  and  $v$  become

$$u = \Re[s - \omega(s)], \quad (23)$$

$$v = \Im[s - \omega(s)]. \quad (24)$$

Using the  $\omega$  function circumvents the detour through troublingly large numbers. To implement  $\omega$  programmatically, a convergent sequence based on Newton's method [9] is used, given by

$$w_{n+1} = w_n - \frac{w_n + \ln(w_n) - z}{1 + \frac{1}{w_n}}. \quad (25)$$

Calculating  $\omega(s)$  for  $\Re(z) < -1000$  risks underflow. Thus, when calculating  $u$  and  $v$ , the following functions are used:

$$W[\exp(s)] \quad \text{if } \psi < 0 \quad \text{and} \quad R_1 \leq \rho \leq R_2, \quad (26)$$

$$\omega(s) \quad \text{otherwise.} \quad (27)$$

To ensure that the correct  $\kappa(z)$  branch of  $W$  is chosen, we check that the resulting value satisfies the relation [10]:

$$W_{\kappa}(z) + \ln[W_{\kappa}(z)] = \ln(z) + 2\pi i \kappa, \quad (28)$$

unless  $\kappa = -1$ ,  $z \in \mathbb{R}$ , and  $-e^{-1} \leq z < 0$ , in which case  $W_{\kappa}(z) + \ln[W_{\kappa}(z)] = \ln(z)$ .

By the symmetry of the Proton EDM experiment geometry, the electric field due to each plate can be calculated individually and the total field can be found by reflecting and rotating accordingly. The spacing is sufficiently large so that the fields of each of the deflector sections can be added directly. The electric field perpendicularity to the plates varies by less than 60  $\mu\text{rad}$  as a result of this addition.

With the Lambert  $W$  and Wright  $\omega$  functions defined and the electric field expressions determined in the previous sections, the electric field can be calculated analytically for any point in the ring.

### C. Particle tracking results

Precision tracking simulations of the Proton EDM lattice using fourth-order Runge-Kutta integration with a step size of 1–10 ps were done recently by Hacıömeroğlu and Semertzidis [11,12] neglecting the deflector fringe fields

and instead using a hard-edge approximation. We implemented a tracking program to account for the fringe effects of the deflectors.

For a particle of mass  $m$  and charge  $e$ , the two differential equations governing particle and spin dynamics for  $\vec{\beta} = \vec{v}/c$  and spin  $\vec{s}$  in external electric and magnetic fields are [13]

$$\frac{d\vec{\beta}}{dt} = \frac{e}{m\gamma c} [\vec{E} + c\vec{\beta} \times \vec{B} - \vec{\beta}(\vec{\beta} \cdot \vec{E})], \quad (29)$$

and the generalized T-BMT equation [14], allowing for a nonzero  $\eta$ , which plays the same role for an electric dipole moment as  $g$  for a magnetic dipole moment, and anomalous magnetic moment  $a$ :

$$\begin{aligned} \frac{d\vec{s}}{dt} = \frac{e}{m} \vec{s} \left[ \left( a + \frac{1}{\gamma} \right) \vec{B} - \frac{a\gamma}{\gamma+1} \vec{\beta}(\vec{\beta} \cdot \vec{B}) - \left( a + \frac{1}{\gamma+1} \right) \frac{\vec{\beta} \times \vec{E}}{c} \right. \\ \left. + \frac{\eta}{2} \left( \frac{\vec{E}}{c} + \vec{\beta} \times \vec{B} - \frac{\gamma}{\gamma+1} \frac{\vec{\beta}(\vec{\beta} \cdot \vec{E})}{c} \right) \right]. \end{aligned} \quad (30)$$

For tracking simulations, we set  $\eta = 0$  and  $\vec{B} = 0$  for an all-electric ring. Fourth-order Runge-Kutta integration was used with a step size of 1–10 ps to numerically solve the two differential equations for a particle in the Proton EDM ring. Energy is conserved to subpart per million levels over the duration of the program. Tracking a particle in an ideal cylindrical ring for 0.2 ms and comparing to analytical values, we find that the errors in the position  $dR/R_0$  and the momentum  $dp/p_0$  were below  $10^{-11}$  for step sizes ranging from 1–100 ps.

The introduction of the geometrical quantity  $\theta$  in the ring accounts for the deflection of the particles toward the center by the nonzero deflector fringe fields in the straight sections. Particles were successfully stored for upwards of 100 turns with a  $\theta$  value of the ring of  $\theta = 1.0$  mrad. Fig. 7 shows the radial oscillations of a stored particle with the design momentum for the first 15  $\mu\text{s}$  of the run.

An important condition for the Proton EDM experiment is to have the spin of the particle aligned with its momentum such that  $\vec{s} \cdot \vec{p}$  is constant on average. Using an angle of  $\theta = 1.0$  mrad, the ideal particle was successfully stored for more than 100 turns with  $\vec{s} \cdot \vec{p}$  constant on average. The spin coherence time  $\tau$  is defined to be the time necessary for the angle between  $\vec{s}$  of the ideal particle and  $\vec{s}_{\text{rms}}$  of the distribution to change by 1 rad. A spin coherence time above  $10^3$  s is within the desired range of the experiment. Using an ensemble of particles with  $(dp/p_0)_{\text{rms}} = 10^{-4}$ , we estimated that the spin coherence time in the ring is consistent with a value on the order of  $10^3$  s.

The dynamic aperture of the simulated ring is shown in Fig. 8 for the  $\theta = 1.0$  mrad that maximizes the spin coherence time of the ideal particle. The aperture illustrates

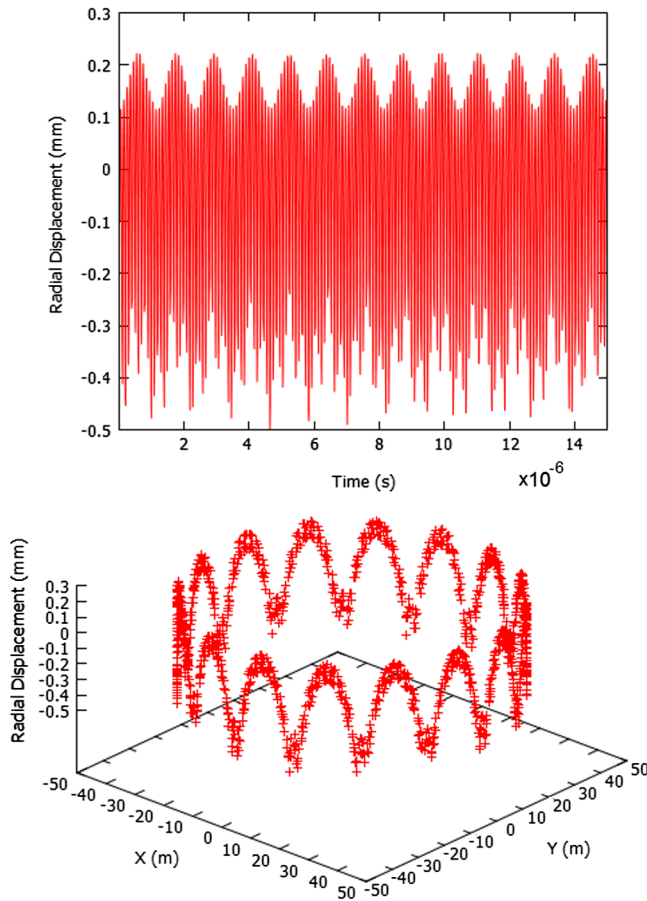


FIG. 7. The radial displacement of a proton with the design momentum around the ring from its hard-edge orbit, starting at an initial position of 45.029 m using an angle  $\theta = 1.0$  mrad. The oscillations about this radius are shown as a function of time (top) and of position around the ring (bottom).

the range of radial deviations  $dR/R_0$  and momentum deviations  $dp/p_0$  of particles that survived more than 100 turns in the ring. The momentum acceptance of the lattice including the deflector fringe fields is well suited to the desired momentum spread  $(dp/p_0)_{rms} = 10^{-4}$  of the particles. The dynamic aperture differs only slightly from the case where fringe fields are neglected. Further, the phase space of particles in the ring, with values taken at the center of a deflector region, is shown in Fig. 9.

Additionally, we introduced a realistic 10 cm radio frequency (rf) cavity in one of the straight sections, with rf equal to 100 times the cyclotron frequency of the ideal particle. We used a peak electric field strength of 5.0 MV/m and included the resulting magnetic field. The rf bucket had a length of 283 cm. The particles behaved as expected with the introduction of the rf in the straight section [12], with no noticeable effect due to the fringe fields.

The present tracking simulation studied the deflector fringe fields in the context of the Proton EDM geometry.

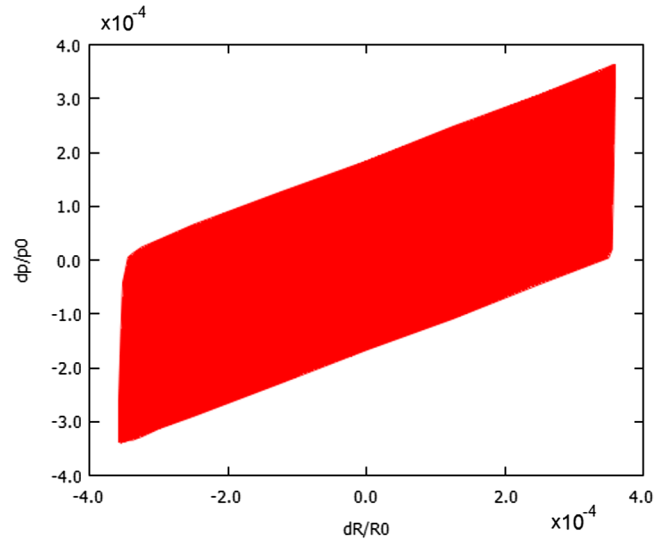


FIG. 8. The dynamic aperture of the ring geometry using  $R_1 = 39.985$  m,  $R_2 = 40.015$  m,  $\ell = 2.0$  m, and  $\theta = 1.0$  mrad. Particles with a momentum deviation  $dp/p_0$  and initial position deviation  $dR/R_0$  in the highlighted region survived more than 100 turns in the ring.

A more complete simulation of the ring including, among other effects, the effects of vertical focusing quadrupoles, alignment tolerances, and counter-rotating particle beams, will be performed in the future, incorporating the present procedure for including the fringe fields of the deflector plates.

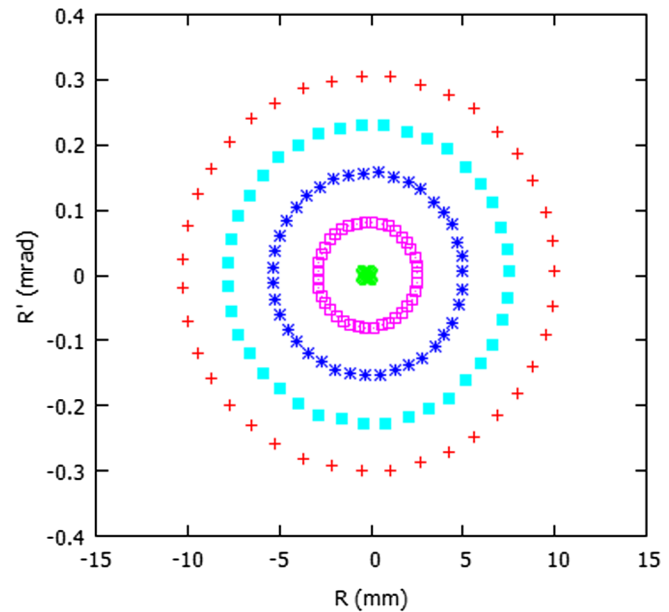


FIG. 9. The phase space of particles in the ring, with values taken at the center of a deflector region, with  $R_1 = 39.985$  m,  $R_2 = 40.015$  m,  $\ell = 2.0$  m, and  $\theta = 1.0$  mrad. The origin of coordinates is taken to be the geometrically central orbit.

## VI. CONCLUSIONS

We have presented an analytic expression for the fringe fields at the end of semi-infinite cylindrical plates extending infinitely in the  $z$  direction in cylindrical coordinates. The implicitly defined  $u$  and  $v$  expressions themselves have utility, with  $[\rho(u, v), \psi(u, v)]$  equipotential lines giving the exact form for Rogowski-profile plates for cylindrical deflectors for any fixed  $v$  value.

Precision tracking simulations using the fourth-order Runge-Kutta method yield that it is possible to store a particle in the Proton EDM deflector geometry of the Proton EDM ring with the spin frozen along the momentum direction, as necessary. The revision of the Proton EDM lattice geometry with 40 m bending radius to include the angle  $\theta = 1.0$  mrad is suggested. A sufficient dynamic aperture and spin coherence time were found with an rf cavity introduced into a straight section. Thus, we have confirmed the feasibility of the proposed model Proton EDM geometry including the fringe electric fields of the deflector plates.

## ACKNOWLEDGMENTS

We would like to thank Ian D'Silva, Marina Fandaros, Brian Gilbert, Danny Huang, Arjun Mehrotra, Divij Sharma, and Andreas Stamatakis for their encouragement and enthusiasm, and Brian Levy for his mathematical discussions. We would also like to thank the Department of Energy and Brookhaven National Laboratory for their continued support of the High School Research Program and the Supplemental Undergraduate Research Program, without which this work would not have been possible. We especially thank the Storage Ring EDM Collaboration.

- [1] J. C. Maxwell, *A Treatise on Electricity and Magnetism* (Clarendon, Oxford, 1873), Vol. 1.
- [2] G. A. Doskeyev, O. A. Edenova, and I. F. Spivak-Lavrov, *Nucl. Instrum. Methods Phys. Res., Sect. A* **645**, 163 (2011).
- [3] R. P. Feynman, R. B. Leighton, and M. L. Sands, *The Feynman Lectures on Physics* (Addison-Wesley, Redwood City, CA, 1989), Vol. 2, Chap. 7, pp. 1–3.
- [4] W. Rogowski, *Archiv Für Elektrotechnik* **12**, 1 (1923).
- [5] S. R. Valluri, D. J. Jeffrey, and R. M. Corless, *Can. J. Phys.* **78**, 823 (2000).
- [6] Storage Ring EDM Collaboration, "A Proposal to Measure the Proton Electric Dipole Moment with  $10^{-29}$  e · cm Sensitivity." October 2011.
- [7] T. R. Scavo and J. B. Thoo, *The American Mathematical Monthly* **102**, 417 (1995).
- [8] R. M. Corless and D. J. Jeffrey, *Proceedings of Artificial Intelligence, Automated Reasoning, and Symbolic Computation, Joint International Conferences, France, 2002* (Springer, Berlin, Heidelberg, 2002).
- [9] J. H. Hubbard and B. B. Hubbard, *Vector Calculus, Linear Algebra, and Differential Forms: A Unified Approach*, 4th ed. (Prentice Hall, Upper Saddle River, NJ, 1999), pp. 232–252.
- [10] D. J. Jeffrey, D. E. G. Hare, and R. M. Corless, *Mathematical Scientist* **21**, 1 (1996).
- [11] S. Hacıömeroğlu and Y. K. Semertzidis, *7th Patras Workshop on Axions, WIMPs and WISPs, 2011* (Deutsches Elektronen-Synchrotron DESY, Hamburg, Germany, 2011).
- [12] S. Hacıömeroğlu and Y. K. Semertzidis, *Nucl. Instrum. Methods Phys. Res., Sect. A* **743**, 96 (2014).
- [13] J. D. Jackson, *Classical Electrodynamics*, 3rd ed. (Wiley, New York, 1998).
- [14] T. Fukuyama and A. J. Silenko, *Int. J. Mod. Phys. A* **28**, 29 (2013).